# Pancreatic β-Cell Failure and Diabetes in Mice With a Deletion Mutation of the Endoplasmic Reticulum Molecular Chaperone Gene P58$^{IPK}$

**Warren C. Ladiges,[1] Sue E. Knoblaugh,[1] John F. Morton,[1] Marcus J. Korth,[2] Bryce L. Sopher,[3] Carole R. Baskin,[1,2] Alasdair MacAuley,[1] Alan G. Goodman,[2] Renee C. LeBoeuf,[4] and Michael G. Katze[2]**

**The endoplasmic reticulum (ER) transmits apoptotic signals in the pancreas during ER stress, implicating ER stress–mediated apoptosis in the development of diabetes. P58$^{IPK}$ (*DNAJC3*) is induced during ER stress and functions as a negative feedback component to inhibit eIF-2α signaling and attenuate the later phases of the ER stress response. To gain insight into a more comprehensive role of P58$^{IPK}$ function, we generated deletion mutant mice that showed a gradual onset of glucosuria and hyperglycemia associated with increasing apoptosis of pancreatic islet cells. Lack of P58$^{IPK}$ had no apparent effect on the functional integrity of viable β-cells. A set of genes associated with apoptosis showed altered expression in pancreatic islets from P58$^{IPK}$-null mice, further substantiating the apoptosis phenotype. The data provide in vivo evidence to support the concept that P58$^{IPK}$ functions as a signal for the downregulation of ER-associated proteins involved in the initial ER stress response, thus preventing excessive cell loss by degradation pathways. Insulin deficiency associated with the absence of P58$^{IPK}$ mimics β-cell failure associated with type 1 and late-stage type 2 diabetes. P58$^{IPK}$ function and activity may therefore provide a novel area of investigation into ER-mediated mechanistic and therapeutic approaches for diabetes. *Diabetes* 54:1074–1081, 2005**

The endoplasmic reticulum (ER) is a signal-transducing organelle in physical and biochemical contact with the nucleus that continuously senses intracellular changes brought about by such conditions as changes in glucose and calcium homeostasis, heat shock, hypoxia, alteration in protein structure due to genetic defects or toxic or endogenous compounds, and protein misfolding caused by endogenous or exogenous compounds (1). The ER stress response is generally defined by increased expression of proteins known to be residents of the ER, such as BiP (GRP78), PERK, and Ire1 as well as other nonresident proteins such as ATF4 and CHOP (GADD153) (2,3). Apoptotic pathways have been described including JNK protein kinase, caspase 12, and ATF4-activated CHOP (4). Several recently characterized mouse models have led to new insights into glucose homeostasis and ER stress. Scheuner et al. (5) generated mice with a homozygous mutation at the eIF-2α phosphorylation site (Ser51Ala). These mice died within 18 h of birth due to hypoglycemia associated with defective gluconeogenesis and defective pancreatic β-cells. Studies with this mouse model demonstrate that translational regulation through eIF-2α phosphorylation is required for the maintenance of blood glucose and pancreatic insulin content. Harding et al. (6) showed that PERK-null mutant mice lose their ability to control translation in response to ER stress. This leads to an inappropriate load on the β-cell ER and a saturation of proteins. Subsequent folding of even a small amount of surplus proteins can allow these proteins to assume abnormal conformations and serve as proteotoxins. The propensity of mice and humans with PERK mutations to develop diabetes suggests that the endocrine pancreas may be especially sensitive to ER stress.

Recent studies have shown that one of the genes consistently induced during ER stress is P58$^{IPK}$ (*DNAJC3*). Van Huizen et al. (7) showed that P58$^{IPK}$ is an important component of a negative feedback loop used by the cell to inhibit eIF-2α signaling and attenuate the unfolded protein response. Studies by Yan et al. (8) suggested that P58$^{IPK}$ induction during ER stress represses PERK and plays a functional role in the expression of downstream markers of PERK activity in the later phase of the ER stress response. PERK is normally activated during the ER stress response to protect cells from ER stress by attenuating protein synthesis and reducing protein load in the ER (3). Cellular stress within the ER activates P58$^{IPK}$ through an ER stress response element in its promoter region, triggering the interaction and inhibition of PERK (8). P58$^{IPK}$ was originally identified as a cellular factor recruited by the influenza virus to downregulate the antiviral activities of the interferon-induced eIF-2α kinase, PKR (9). Intrigu-

From the [1]Department of Comparative Medicine, Comparative Mouse Genomics Center, University of Washington, Seattle, Washington; the [2]Department of Microbiology, University of Washington, Seattle, Washington; the [3]Department of Laboratory Medicine, University of Washington, Seattle, Washington; and the [4]Department of Pathobiology, University of Washington, Seattle, Washington.

Address correspondence and reprint requests to Warren C. Ladiges, Department of Comparative Medicine, Box 357190, University of Washington, Seattle, WA 98195. E-mail: wladiges@u.washington.edu.

Received for publication 20 July 2004 and accepted in revised form 7 January 2005.

AUC, area under the curve; ER, endoplasmic reticulum; GTT, glucose tolerance test; MRS, magnetic resonance spectroscopy.

ingly, the recruitment of P58$^{IPK}$ by viruses may be related to its role as an ER stress response protein, since it is likely that the synthesis of large amounts of viral proteins during viral replication places a major stress upon the ER (10). P58$^{IPK}$ is a member of the tetratricopeptide repeat family of proteins (11), and its COOH-terminal portion shares homology with the J region of the DNAJ heat shock protein of *E. coli*, placing it within the heat shock protein 40 family. It is expressed in all tissues examined in mice and humans, with especially high levels in pancreas and liver (12) and with increased expression in tissues from old mice (13).

To gain a more comprehensive understanding of P58$^{IPK}$ function, we generated deletion mutant mice and demonstrated absence of gene product and a loss of function. We report here our initial observations in P58$^{IPK}$-null mice, which exhibit a gradual onset of increased pancreatic β-cell death and a phenotypic perturbation in glucose homeostasis.

## RESEARCH DESIGN AND METHODS

**Generation of P58$^{IPK}$-deficient embryonic stem cells and mice.** A mouse C57BL/6 genomic DNA library (Genome Systems) in the pBeloBAC11 vector was screened using a restriction fragment probe corresponding to nucleotides −100 to +360 of the mouse P58$^{IPK}$ cDNA (11). Based upon preliminary Southern blot analyses, a 15-kb *Hpa*I fragment was subcloned, restriction mapped, and partially sequenced. This sequence was then assembled into an *actin*/enhanced green fluorescent protein/β-galactosidase/PKG-Neo/pA–targeting vector designed to replace P58$^{IPK}$ exon 1 containing the translation start site. The targeting vector was transfected into C57BL/6-derived embryonic stem cells (14,15). Positive clones were screened by Southern and PCR and microinjected into 3.5-day-old blastocysts isolated from BALB/c mice. The contribution of these stem cells to the germline of chimeric mice was assessed by breeding with C57BL/6 females and screening for black offspring. Heterozygous mice were identified by PCR and intercrossed to obtain a Mendelian ratio of homozygous offspring. Routine genotyping for homozygosity was done by PCR using two sets of primers specific for an internal targeting deletion sequence (flanking the 59-bp *Xmal* deletion in the targeted P58$^{IPK}$ allele) and an external genomic sequence. Mice were 100% C57BL/6 (from a C57BL/6 embryonic stem cell line) and were maintained on the C57BL/6 background by alternate generation backcrossing. Mice were maintained in a specific pathogen-free barrier facility with standard rodent diet and 12-h alternating light and dark cycles. All experiments were approved by the University of Washington Institutional Animal Care and Use Committee.

**Clinical chemistry assays.** Blood glucose levels were measured with a portable glucose measuring device (Accu-Chek Advantage). Glucose values read from 10 to 600 mg/dl. Urine glucose and ketones were measured with urinalysis reagent strips (Keto-Diastix) from Bayer. Serum insulin levels were measured by radioimmunoassay (Phoenix Central Laboratory, Everett, WA) and total plasma triglycerides by Triglyceride/GB kit no. 450032 (Roche Diagnostics).

**Histological analysis and immunohistochemistry.** Fixed pancreata, as well as other organs and tissues, were trimmed, embedded in paraffin, sectioned, stained with hematoxylin and eosin, and examined microscopically. Immunohistochemistry was performed on tissue fixed in 10% neutral buffered formalin overnight. Slides were steamed in citrate buffer for 10 min for antigen retrieval. Guinea pig anti-insulin primary antibody (Fitzgerald Labs) diluted 1:450 and rabbit anti-glucagon primary antibody (Vector Labs) diluted 1:30 were used. Biotinylated anti-guinea pig and anti-rabbit secondary antibodies and the Vectastain ABC kit (Vector Labs) were used for secondary staining and color development. The caspase 3 assay for apoptosis was performed by using primary rabbit anti-cleaved caspase 3 antibody (Cell Signaling Technologies) diluted at 1:200 and biotinylated anti-rabbit secondary as already described.

**Glucose tolerance test and insulin sensitivity assays.** For the glucose tolerance test (GTT), mice were fasted overnight (14 h) and injected intraperitoneally with 10% glucose in PBS at a dose of 2 g glucose/kg body wt. Plasma glucose was monitored before glucose injection and at 30, 60, 120, and 240 min after injection. Glucose values were normalized to percent initial glucose by calculating the ratio of challenge values versus prechallenge values at each time point (16). For the insulin sensitivity assay, mice were fasted overnight and injected intraperitoneally with 0.1 units/ml Humulin R insulin (Lilly) in sterile PBS at a dose of 1.0 units insulin/kg body wt. Plasma glucose was monitored before and 30 min after insulin injection. The percentage decrease in glucose between these time points was then calculated as follows: % glucose disposed = [(glucose$_{t=0}$ − glucose$_{t=30}$)/glucose$_{t=0}$] × 100 (17).

**Quantitation of adiposity.** Body composition was assessed using whole-body magnetic resonance spectroscopy (MRS) as described (16,18). Mice were anesthetized with ketamine/zylazine, secured within a radio frequency coil for transmitting and receiving the resonant proton signal at 200.1 MHz, and scanned using a 4.7-T magnet (Bruker). Magnetic field inhomogeneities were corrected by hand shim adjustment before each spectral acquisition, and three acquisitions were obtained per animal. Each mouse was carefully centered within the coil, and the coil was placed at exactly the same longitudinal and rotational position for each reading. Areas under the curve (AUCs) were obtained for water and lipids using line integrals (Verizu, Palo Alto, CA). The AUC for the water peak was demarcated by the region from 10 ppm to the relative minimum transformed signal between the water and the lipid peak. The AUC for the lipid peak was demarcated by the same relative minimum between peaks and −3 ppm.

**Pancreatic islet cell isolation.** Pancreatic islets were harvested from anesthetized mice by the Islet Cell and Functional Analysis Core of the Diabetes Endocrinology Research Center at the University of Washington as previously described (19). Briefly, islets were prepared by injecting collagenase (2 ml of 0.23 mg/ml liberase; Roche Molecular Biochemicals, Indianapolis, IN) into the pancreatic duct and surgically removing the pancreas. The pancreas was then placed in a 15-ml conical tube containing 5 ml of 0.23 mg/ml liberase and incubated at 37° for 30 min. The digestate was filtered (400-μg stainless steel screen), rinsed in Hank's buffered salt solution, and purified in a gradient of Optiprep (Nycomed, Osh, Norway). Islets were hand picked, rinsed, and immediately frozen for mRNA isolation. A routine harvest from an adult male wild-type C57BL/6 mouse typically yields about 120 islets.

**Gene expression assay of pancreatic islets.** Total RNA from isolated islets was purified, reverse transcribed, and amplified. The resulting cDNA from each P58$^{IPK}$-null sample and pooled P58$^{IPK}$ wild-type samples were labeled with two different dyes (Cy3 and Cy5) in duplicate, resulting in four separate measurements for each gene on the array. This allowed for calculation of a mean ratio and an SD of the ratio, which was used as an error estimate. The mouse cDNA arrays were made by the Center for Expression Arrays at the University of Washington and contained duplicate spots of 6,913 unique cDNA clones. Total gene lists of signature genes ($P \leq 0.05$) in all arrays were generated in Resolver and clustered according to a bioset of genes associated in some way with apoptotic pathways. Each cluster was generated with a hierarchical algorithm (fold change >1.5 and $P \leq 0.05$ in at least two experiments) using Spotfire Decision Site 7.1.1. The premise of the clustering approach is that genes having similar expression profiles across a set of conditions may share similar functions. Genes were further clustered into the functional category of apoptosis as defined by the gene ontology resource known as FatiGO (fast transference of information using gene ontology; available at http://fatigo.bioinfo.cnio.es/).

## RESULTS

**Generation of P58$^{IPK}$-null mice.** The overall strategy for making P58$^{IPK}$ knockout mice is outlined in Fig. 1*A*. Five P58$^{IPK}$ enhanced green fluorescent protein clones were injected into blastocysts and used to derive chimeric mice by previously described procedures (14). Germ line transmission was achieved with two of the clones. Mice were intercrossed within each line to generate homozygous progeny. Genotype assignments were made by PCR as already described. Tissues and embryonic fibroblasts derived from homozygous, heterozygous, and wild-type littermates were processed and subjected to Western blot analysis (Fig. 1*B*). All progeny displayed the expected Mendelian ratio of heterozygous versus homozygous genotypes.

**Growth and development of P58$^{IPK}$-null mice.** The P58$^{IPK}$-null deletion mutation did not affect breeding fecundity, since both males and females breed normally and litter sizes were similar in all genotypes. However, null mice are smaller and can be easily distinguished from heterozygous and wild-type mice at as early as 2 weeks of age. Growth curves beginning at 8 weeks of age show that body weights of null mice increase in parallel but never

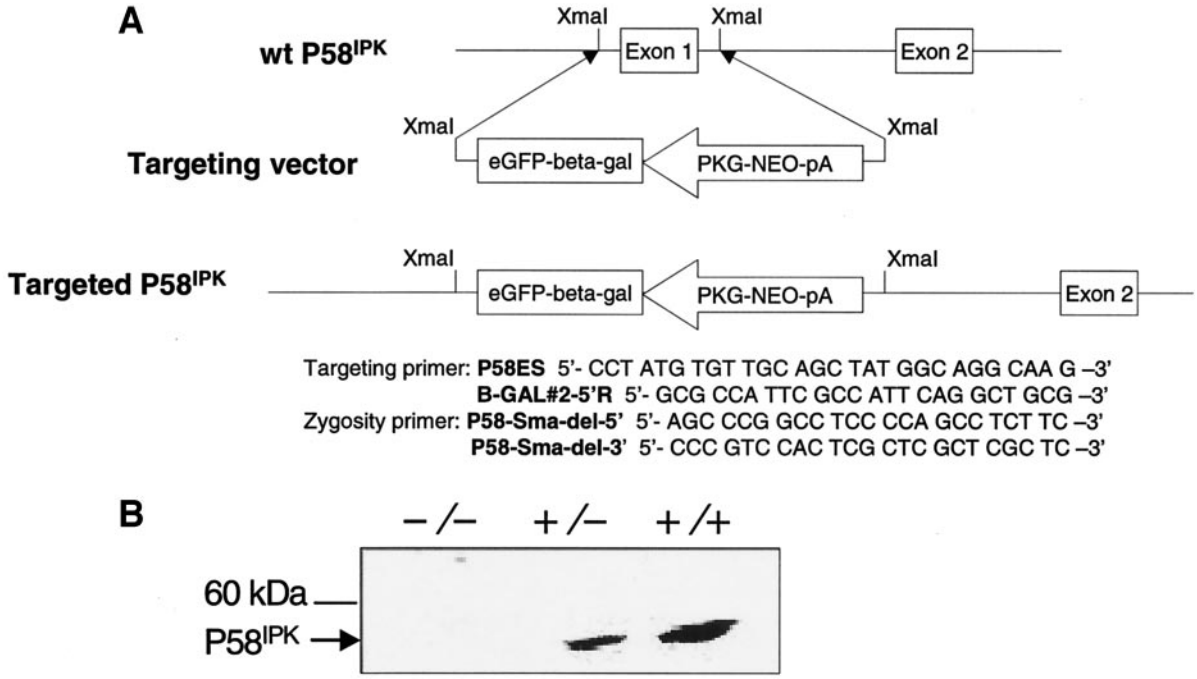


**FIG. 1. Generation of P58IPK-null mice. *A*: P58IPK-targeting vector strategy, with details described in the text. The genotyping primer sequences are shown. A C57BL/6 ES cell line was used for targeting so all mice are 100% B6 background. *B*: Western blot analysis of cellular lysates from P58IPK-null (*lane 1*), P58IPK heterozygous (*lane 2*), and wild-type (*lane 3*) embryonic fibroblasts.**

catch up to the heterozygous or wild-type genotype. This phenotype is more pronounced in male than female mice, although it is still apparent in females (Figs. 2*A* and *B*, respectively). P58IPK-null males have an average life span of 14.5 months. Female null mice, as well as heterozygous male and female mice, live longer, but it has not yet been determined if they have life spans different from wild-type C57BL/6 mice (25 months).

To investigate the cause of the lower body weight in null mice, we measured organ weights, and these were generally within normal range (data not shown). However, a striking observation at necropsy was very little body fat. Body fat percentage was determined in a subset of 10- to 12-month-old male mice by using MRS. Figure 3*A* shows a scan for a wild-type littermate, where the left peak represents the aqueous percentage and the right peak represents the lipid percentage. Figure 3*B* shows an MRS scan for a P58IPK-null mouse, with an absence of the right peak indicating diminished body fat stores. The average calculated percent body fat for each of two null mice was 7% compared with an average percent body fat of 34% for each of two wild-type control mice. Once null mice reach their mature weight, they maintain this weight and do not gain additional weight as wild-type mice do. Heterozygous mice, as well as female null mice, appear to behave similar to null males in maintaining their weight as they age. We have documented that the paucity of fat stores is not due to decreased food intake. In two separate feeding experiments, we measured food intake by cohorts of five mice each for 7 days and calculated total intake per gram body weight. Wild-type and heterozygous mice consumed an average of 2.8 and 3 grams of food per gram body weight, respectively, over the 7-day period. Null mice consumed an average of 4.4 grams of food per gram of body weight.

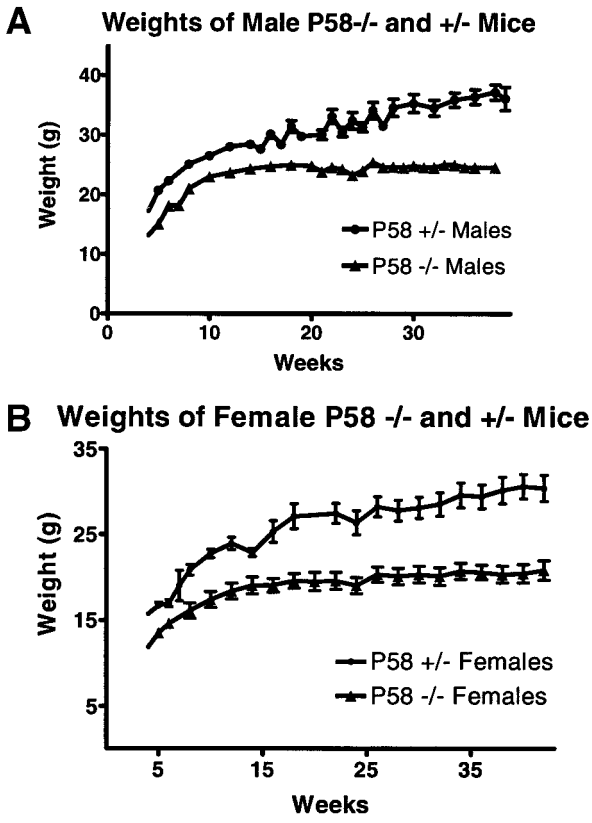


**FIG. 2. Body weights. *A*: Body weights of male P58IPK-null and P58IPK heterozygous mice from 4 to 40 weeks of age with an average of 10 mice per data point. *B*: Body weights of female P58IPK-null and P58IPK heterozygous mice from 4 to 40 weeks of age with an average of seven mice per data point.**

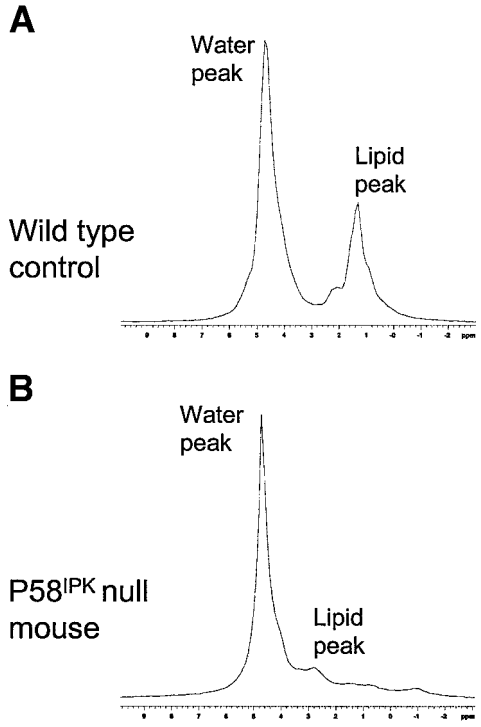


**FIG. 3. MRS. Three scanning acquisitions were obtained for each of four male mice, two null and two wild-type, under light ketamine/xylaxine anesthesia. AUCs were obtained for water and lipid using line integrals (Verizu). The AUC for the water peak was demarcated by the region from 10 ppm to the relative minimum transformed signal between the water and the lipid peak. The AUC for the lipid peak was demarcated by the same relative minimum between peaks and −3 ppm. The scan is representative of all scans obtained from both pairs of mice representing wild-type (*A*) and null (*B*).**

**P58$^{IPK}$-null mice display glucosuria, hyperglycemia, and hypoinsulinemia.** As mice reached adult maturity (4 months of age), they began increasing their water intake with subsequent increased urination and evidence of glucosuria, with values increasing as mice became older (data not shown). Serum glucose levels were shown to be higher than normal (Fig. 4*A*) in parallel with urine glucose values. The same P58$^{IPK}$-null mice also developed hypoinsulinemia compared with wild-type control littermates (Fig. 4*B*). It is interesting to note, however, that mice were not outwardly sick. None of the mice showed any evidence of urine ketones (data not shown), suggesting that there was adequate compensation for the gradual onset of diabetes.

We investigated whether the hyperglycemia in P58$^{IPK}$-null mice might be the result of insulin resistance by performing a GTT and an insulin sensitivity assay in pre-diabetic mice. The GTT was performed by injecting glucose into 8-week-old fasted mice and determining blood glucose levels and time required for stabilization to basal levels. We showed that blood glucose response patterns and times to return to basal levels after 240 min were similar in null and wild-type mice (Fig. 4*C*). The normalized curves (percent initial glucose load) showed that the P58$^{IPK}$-null mice were insulin sensitive, even though at 60 min relative glucose excursion was reduced compared with wild type. To directly assess glucose clearance, we performed in vivo insulin-mediated glucose disposal assays in the same pre-diabetic cohort. Glucose clearance was equally efficient in both null and wild-type littermate control mice, with 29 and 33% clearance, respectively (Fig. 4*D*). These experiments showed that P58$^{IPK}$-null mice were not insulin resistant, since they cleared glucose just as efficiently as wild-type controls when challenged with a standard glucose load. It was also apparent that pre-diabetic P58$^{IPK}$-null mice were capable of responding to insulin, suggesting that viable β-cells from these mutant mice are functional.

**P58$^{IPK}$-null mice show pancreatic β-cell depletion.** We looked at histological sections of pancreata and saw altered morphology in adult male mice as they first presented with hyperglycemia. Figure 5*B* shows typical pathological morphology of islets in a 6-month-old male P58$^{IPK}$-null mouse compared with normal islet morphology in an age-matched wild-type male mouse (Fig. 5*A*). There was cytoplasmic atrophy and collapse within the pancreatic islets, which gave the appearance of an increase in nuclear density. Multifocal areas of cytoplasmic clefts and apoptotic bodies were also found. These pathological changes were limited to the islets, with no evidence of histological changes in acini or other parenchyma and no signs of inflammatory infiltration. Pancreatic β-cell lesions were seen as early as 3 months of age.

We stained paraffin-fixed pancreatic sections with anti-insulin antibody to determine the relative presence of insulin in P58$^{IPK}$-null mouse pancreatic islets. As can be seen in Fig. 5*C*, islets from wild-type littermates had intense staining throughout the islet parenchyma, while islets from P58$^{IPK}$-null mice (Fig. 5*D*) showed a sparse scattered staining pattern suggesting low insulin levels and decreased number of β-cells. Anti-glucagon antibody revealed staining of α-cells in the mantle of the islets in the control wild-type mice (Fig. 5*E*), while islets from P58$^{IPK}$-null mice had more intense or darker stain in the mantle as well as some staining in the core of the islet (Fig. 5*F*). In conclusion, the mass of insulin-producing cells was significantly decreased in the islets of the P58$^{IPK}$-null mice, while the glucagon-producing cells were found in the core as well as the mantle of the islets.

**Pancreatic β-cell failure in P58$^{IPK}$-null mice is associated with increased apoptosis and upregulation of genes associated with apoptosis.** A possible reason for the hypoinsulinemia in P58$^{IPK}$-null mice might be due to increased β-cell death as the result of increased ER stress, i.e., adequate numbers of β-cells are being generated but large numbers are being eliminated by apoptosis. We stained paraffin-fixed pancreatic sections in a cleaved caspase 3 assay and showed increased apoptosis in islets from null mice (Fig. 6*B*) but not wild-type littermates (Fig. 6*A*). To complement the cleaved caspase 3 experiment and obtain a broader view of the apoptotic pathway in P58$^{IPK}$-null mice, we performed gene expression analysis on isolated pancreatic islet cells, comparing islets from three null male mice, 4–5 months of age, to islets from age- and sex-matched wild-type mice. Of 886 genes behaving differently between the pancreatic islets of P58$^{IPK}$-null and P58$^{IPK}$ wild-type mice (fold change $\geq$1.5, $P \leq 0.05$), 576 had higher levels of expression in the P58$^{IPK}$-null islets than in the wild-type islets, and 310 had lower levels of expression. Using FatiGO, 20 genes were clustered into the functional category of apoptosis (Fig. 6*C*), further supporting the histological find-

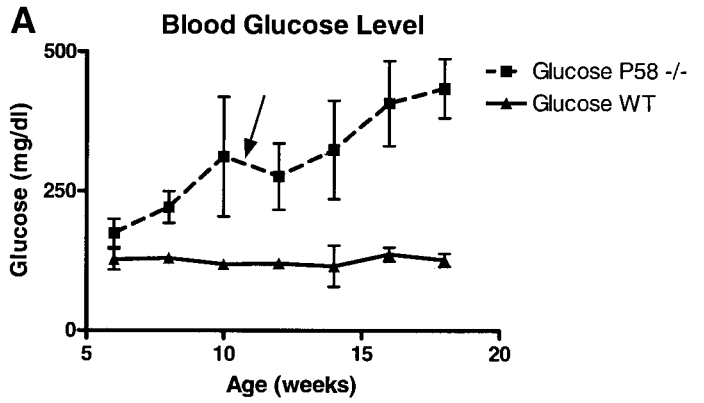


B

| Age (weeks) | Serum insulin (ng/ml) P58$^{IPK}$ null | Serum insulin (ng/ml) Wild type |
|---|---|---|
| 8 | 02.5±0.6 | 4.8±1.8 |
| 16 | 0.9±0.1* | 8.1±3.2* |
| 44 | <0.5* | 27.8±13.7* |

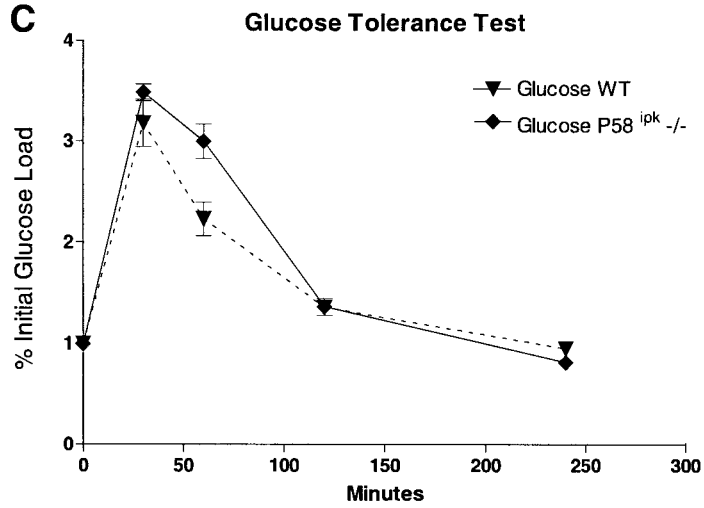


D

| Serum glucose | P58$^{IPK}$ null mice | Wild type mice |
|---|---|---|
| % clearance | 31±8 | 24±4 |

**FIG. 4. Glucose homeostasis in P58$^{IPK}$-null male mice. *A*: Nonfasted blood glucose levels representing an average of five mice per cohort at each time point. *B*: Nonfasted serum insulin levels in the same cohort of mice as for 4*A*. *Differences were significant ($P \leq 0.01$) at 16 weeks. *C*: GTT. Five mice per cohort in two separate experiments were fasted overnight and injected intraperitoneally with 10% glucose in PBS at a dose of 2 g glucose/kg body wt. Mice were 8 weeks of age. *D*: Average percent glucose clearance at 30 min following challenge with insulin (1.0 unit/kg body wt) in the same fasted mouse cohorts as for 4*C*. The difference was not significant.**

ings and apoptotic assay that showed increased cell death in islets from P58$^{IPK}$-null mice.

## DISCUSSION

We have shown that deletion of the ER stress–induced molecular chaperone gene P58$^{IPK}$ in the mouse results in several biological phenotypes. Decreased adiposity, resulting in low body weights, was documented by MRS, showing that P58$^{IPK}$-null mice have <10% body fat even at an older age of 10–12 months on an ad libitum diet. The mechanism for the low body fat is possibly due to the early onset of β-cell destruction and decrease in available insulin, preventing the conversion of glucose to fat stores. It is also possible that the hypoinsulinemia caused a downregulation of lipoprotein lipase, resulting in a reduction of circulating triglycerides and subsequent reduction of fatty acid uptake into adipocytes. Total plasma triglyceride levels were not significantly different in wild-type mice versus null mice (data not shown), so this may be less of a possibility.

The hyperglycemia phenotype appears to be related to hypoinsulinemia. The normalized curves for the GTT showed that the P58$^{IPK}$-null mouse is insulin sensitive, since blood glucose levels returned to basal levels just as efficiently as the wild-type control mice. This suggested that some mechanism other than insulin resistance might be responsible for the hypoinsulinemia. Apoptosis in β-cells is involved in both type 1 and type 2 diabetes (21). Recent studies have shown that the ER can transmit apoptotic signals during the ER stress response (22) and implicates ER stress–mediated apoptosis in the development of both type 1 and type 2 diabetes. We speculated that adequate numbers of β-cells were being generated in our P58$^{IPK}$-null mice, but large numbers were being eliminated by apoptosis as a result of increased ER stress. We have preliminary evidence (data not shown) that pooled islets collected from 6-month-old P58$^{IPK}$-null mice cultured in 2 or 20 mmol/l glucose medium have a 10-fold decrease in insulin content compared with islets from age-matched wild-type control mice. Although additional studies are warranted, this observation does suggest support for a specific decrease in β-cell mass.

We subsequently showed, using immunohistological stains, that insulin-producing β-cells, but not glucagon producing cells, were greatly depleted in pancreatic islets from P58$^{IPK}$-null mice, confirming our initial observations of hypoinsulinemia. This depletion was associated with increased apoptosis, since caspase activity was increased in islets from P58$^{IPK}$-null mice compared with wild-type

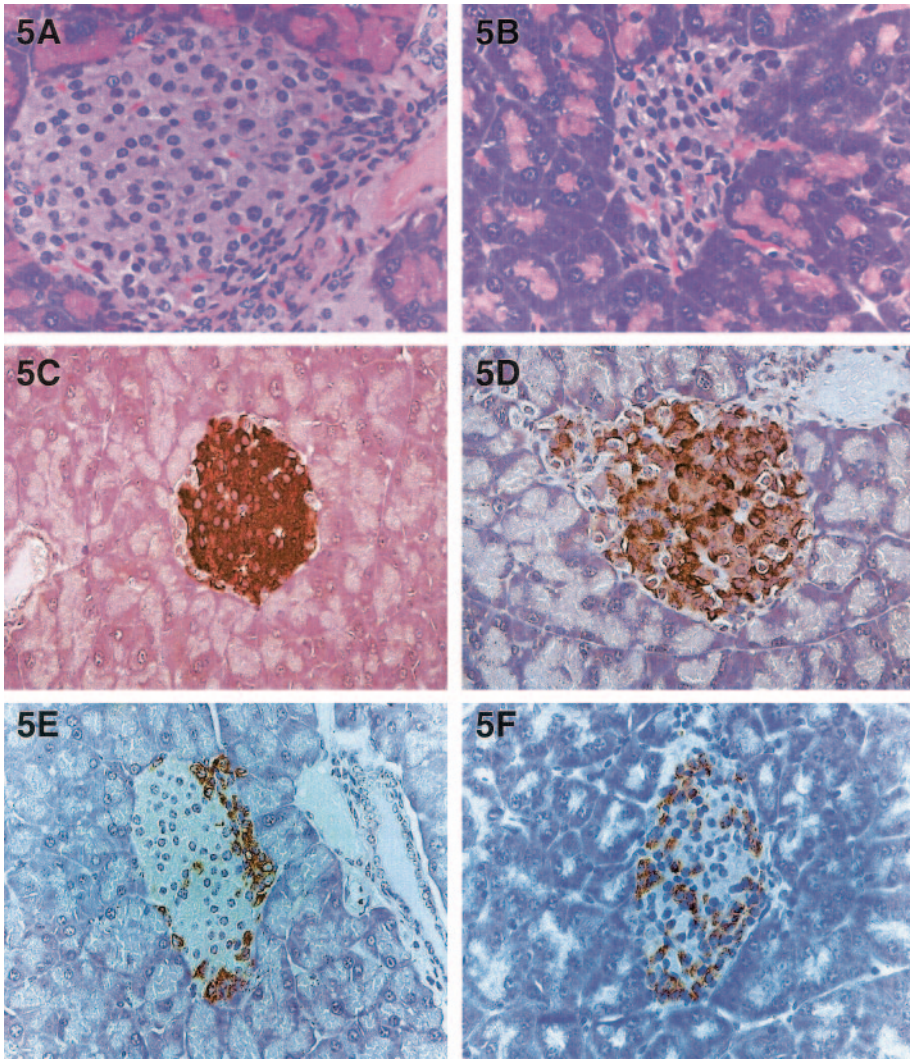


**FIG. 5. Representative histological and immunohistochemical analysis of formalin-fixed pancreatic sections from male mice 4–5 months of age. All sections are at 400× magnification. Hematoxylin and eosin stain for wild-type (*A*) and P58$^{IPK}$-null (*B*) mice. Anti-insulin immunohistochemistry stain for wild-type (*C*) and P58$^{IPK}$-null (*D*) mice. Anti-glucagon immunohistochemistry for wild-type (*E*) and P58$^{IPK}$-null (*F*) mice.**

mice. Caspase 3 is the downstream effector caspase of several apoptotic pathways. Caspase 12 is triggered by ER stress and subsequently activates caspase 3 (23). Since it has been shown that ATF4 induces expression of CHOP (24), this might be another possible mechanism of apoptotic enhancement in P58$^{IPK}$-null mice. PERK-phosphorylated eIF-2α can selectively increase mRNA levels of ATF4 (24), and since PERK is in an active state in the absence of P58$^{IPK}$ (8), the long-term presence of phosphorylated eIF-2α may be an overriding stimulus triggering apoptosis by as yet unidentified pathways. Release of calcium from the ER during the ER stress response might represent an additional mechanism for initiating apoptosis. Any of the genes identified as expression regulated (Fig. 6*C*) could be associated with P58$^{IPK}$ in influencing apoptotic pathways. With the recent finding that ER stress prevents p53-dependent apoptosis (25), it is of interest to see that the p53 apoptosis–associated target gene (PERP) is identified in the array data. The increased expression of lysosomal enzyme genes (cathepsins) is intriguing and worthy of further investigation.

The moderate diabetic phenotype of the P58$^{IPK}$-null mouse model is in contrast to the eIF-2α–mediated mouse models (PERK-targeted deletion mutant and eIF-2α–targeted insertion mutant) recently described (5,6). Both these mouse models have severe phenotypes, with disruption of glucose homeostasis early in neonatal life and numerous other life-threatening pathologies. The eIF-2α Ser51Leu mutant mice have an apparent developmental defect in pancreatic β-cells, whereas P58$^{IPK}$-null mice have functional β-cells that are gradually depleted later as mice become older. PERK-null mice lack the ability to modulate protein synthesis in response to glucose-mediated stimulation of proinsulin (26). As a consequence, proinsulin levels increase in the ER, exceeding its folding capacity and resulting in toxic configurations that most likely deteriorate β-cell integrity. PERK-null mice die soon after birth, indicating a severe phenotype that is probably related to additional vital biological functions of the PERK protein. The less severe phenotype in P58$^{IPK}$-null mice may be related to the fact that P58$^{IPK}$ is not directly involved in controlling protein translation, whereas eIF-2α and PERK are key players in this vital process. These two genes have a major impact on protein synthesis not only in the endocrine pancreas but other tissues and organs as well. In addition, the very high levels of P58$^{IPK}$ protein in the pancreas compared with other tissues (13) may suggest this gene has a unique role in the ER-mediated regulation of glucose homeostasis with less impact on gene function in other tissues. Although we have not yet identified the

A

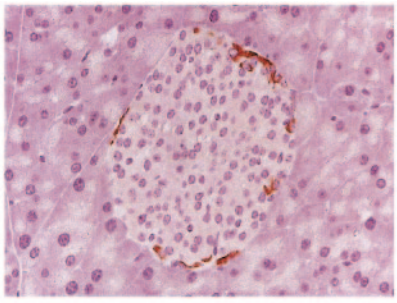

B

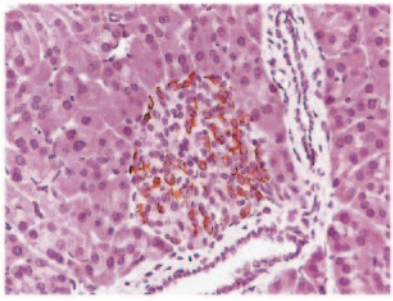

C

| Gene name | Fold change | Description |
|---|---|---|
| Cathepsin L | 4.0 | Lysosomal-mediated apoptosis |
| PERP | 3.8 | P53 apoptosis-associated target |
| PARM1 | 3.1 | Prostate apoptosis related |
| LTBR | 2.5 | Lymphotoxin B receptor |
| Cathepsin D | 2.0 | Lysosomal-mediated apoptosis |
| Cathepsin B | 1.9 | Lysosomal-mediated apoptosis |
| OMI | 1.8 | RNA mediated apoptosis |
| RNASE6PL | 1.8 | Ribonuclease 6 precursor |
| RAI3 | 1.7 | Retinoic acid induced apoptosis |
| BAG3 | 1.7 | Anti-apoptotic factor |
| FASL | 1.7 | Induction of apoptosis |
| Cathepsin Z | 1.7 | Lysosomal-mediated apoptosis |
| IRF5 | 1.7 | Interferon regulatory factor 5 |
| BCAP31 | 1.6 | ER mediated apoptosis |
| Annexin1 | 1.6 | Pro-apoptotic factor |
| CYCS | 1.5 | Cytochrome C |
| Beta arrestin2 | -1.6 | Inhibition of NFKB |
| Stat3 | -1.6 | Inhibition of apoptosis |
| TIA1 | -1.8 | RNA pro-apoptotic factor |
| NFKB1 | -2.1 | Anti-apoptotic function |

**FIG. 6. Caspase 3 apoptosis and proapototic gene expression. Cleaved caspase 3 immunohistochemistry stain for apoptosis at 400× representing wild-type (*A*) and P58IPK-null (*B*) mice 4–5 months of age. *C*: Expression of genes associated with apoptosis in P58IPK-null diabetic versus wild-type islet cell cDNA representing three separate mouse cohorts, aged 4–5 months. Genes differentially regulated by 1.5-fold or greater in at least two experiments ($P \leq 0.05$) were clustered into the functional category of apoptosis as defined by the gene ontology resource known as FatiGO (fast transference of information using Gene Ontology; available at http://fatigo.bioinfo.cnio.es/). Since FatiGO performs analysis on nodes of gene ontology hierarchy, any gene annotated as apoptosis or resulting in apoptosis was considered in the same category.**

specific mechanism responsible for the development of diabetes in P58IPK-null mice, the phenotype clearly distinguishes it from either of the above two mouse lines and provides a model more amenable to longitudinal studies of the ER stress response.

Based on our observations, we suggest that P58IPK plays a role in the ER stress response by functioning as an "off switch" to signal downregulation of ER resident proteins involved in the initial stress response. The ultimate result of a lack of P58IPK in the pancreas is a gradual onset of deficiency of insulin, which mimics β-cell failure associated with type 1 and late-stage type 2 diabetes. The role of the ER stress response in the development and progression of diabetes has not yet been clearly established (26), but P58IPK function and activity may provide a novel area of investigation into ER-mediated mechanistic and therapeutic approaches for this epidemic disease.

## ACKNOWLEDGMENTS

This work was supported by National Institutes of Health Grants U01ES11045 (to W.L.), R01AI22646 (to M.K.), P30ES0703 (to W.L.), and HL52848 (to R.L.).

We thank Ruby Mangalindan and Ashot Safarli for their outstanding efforts in maintaining the mouse colony and assisting with the animal experiments and Dr. Ian Sweet and the Islet Cell and Functional Analysis Core in the Diabetes Endocrinology Research Center, University of Washington (funded by P30DK17047), for islet cell collection. We thank Tim McMillen for performing triglyceride assays.

## REFERENCES

1. Kaufman RJ: Orchestrating the unfolded protein response in health and disease. *J Clin Invest* 110:1389–1398, 2002
2. Iwawaki T, Akai R, Kohno K, Miura M: A transgenic mouse model for monitoring endoplasmic reticulum stress. *Nat Med* 10:98–102, 2004
3. Ron D: Translational control in the endoplasmic reticulum. *J Clin Invest* 110:1383–1388, 2002
4. Zhang K, Kaufman RJ: Signaling the unfolded protein response from the endoplasmic reticulum. *J Biol Chem* 279:25935–25938, 2004
5. Scheuner DS, Song B, McEwen E, Liu C, Laybutt R, Gillespie P, Saunders T, Bonner-Weir S, Kaufman RJ: Translational control is required for the unfolded protein response and in vivo glucose homeostasis. *Mol Cell* 7:1165–1176, 2001
6. Harding HP, Zhang Y, Bertolotti A, Zeng H, Ron D: Perk is essential for

translational regulation and cell survival during the unfolded protein response. *Mol Cell* 5:897–904, 2000
7. van Huizen R, Martindale JL, Gorospe M, Holbrook NJ: P58IPK, a novel endoplasmic reticulum stress-inducible protein and potential negative regulator of eIF2alpha signaling. *J Biol Chem* 278:15558–15564, 2003
8. Yan W, Frank CL, Korth MJ, Sopher BL, Novoa I, Ron D, Katze MG: Control of PERK eIF2alpha kinase activity by the endoplasmic reticulum stress-induced molecular chaperone P58IPK. *Proc Natl Acad Sci U S A* 99:15920–15925, 2002
9. Lee TG, Tomita J, Hovanessian AG, Katze MG: Purification and partial characterization of a cellular inhibitor of the interferon-induced protein kinase of $M_r$ 68,000 from influenza virus-infected cells. *Proc Natl Acad Sci USA* 87:6208–6212, 1990
10. Katze MG, He Y, Gale M Jr: Viruses and interferon: a fight for supremacy. *Nat Rev Immunol* 2:675–687, 2002
11. Lee TG, Tang N, Thompson S, Miller J, Katze MG: The 58,000-dalton cellular inhibitor of the interferon-induced double-stranded RNA-activated protein kinase (PKR) is a member of the tetratricopeptide repeat family of proteins. *Mol Cell Biol* 14:2331–2342, 1994
12. Korth MJ, Lyons CN, Wambach M, Katze MG: Cloning, expression, and cellular localization of the oncogenic 58-kDa inhibitor of the RNA-activated human and mouse protein kinase. *Gene* 170:181–188, 1996
13. Ladiges W, Morton J, Filley G, Hopkins H, Ware C, Gale M: Expression of human PKR protein kinase in transgenic mice. *J Interferon Cytokine Res* 22:329–334, 2002
14. Ladiges WC, Ware CB: Transgenic animals in toxicology. In *Current Protocols in Toxicology*. Maines M, Ed. New York, John Wiley and Sons, 1999
15. Ware CB, Siverts LA, Nelson AM, Morton JF, Ladiges WC: Utility of a C57BL/6 ES line versus 129 ES lines for targeted mutations in mice. *Transgenic Res* 12:743–746, 2003
16. Schreyer SA, Vick C, Lystig TC, Mystkowski P, LeBoeuf RC: LDL receptor but not apolipoprotein E deficiency increases diet-induced obesity and diabetes in mice. *Am J Physiol Endocrinol Metab* 282:E207–E214, 2002
17. Schreyer SA, Cummings DE, McKnight GS, LeBoeuf RC: Mutation of the RIIβ subunit of protein kinase A prevents diet-induced insulin resistance and dyslipidemia in mice. *Diabetes* 50:2555–2562, 2001
18. Mystokowski P, Shankland E, Scheyer SA, LeBoeuf RC, Scwartz RS, Cummings DE, Kushmerick M, Schwartz MW: Validation of whole-body magnetic resonance as a tool to assess murine body composition. *Intl J Obesity* 24:719–724, 2000
19. Sweet IR, Cook DL, DeJulio E, Wallen AR, Khalil G, Callis J, Reems J: Regulation of ATP/ADP in pancreatic islets. *Diabetes* 53:401–409, 2004
20. Tang NM, Korth MJ, Gale M Jr, Wambach M, Der SD, Bandyopadhyay SK, Williams BRG, Katze MG: Inhibition of double-stranded RNA- and tumor necrosis factor alpha-medicated apoptosis by tetratricopeptide repeat protein and cochaperone $P58^{IPK}$. *Molec Cell Biol* 19:4757–4765, 1999
21. Donath MY, Halban PA: Decreased beta-cell mass in diabetes: significance, mechanisms and therapeutic implications. *Diabetologia* 47:581–589, 2004
22. Araki E, Oyadomari S, Mori M: Impact of endoplasmic reticulum stress pathway on pancreatic beta-cells and diabetes mellitus. *Exp Biol Med* 228:1213–1217, 2003
23. Hitomi J, Katayama T, Taniguchi M, Honda A, Imaizumi K, Tohyama M: Apoptosis induced by endoplasmic reticulum stress depends on activation of caspase-3 via caspase-12. *Neurosci Lett* 357:127–130, 2004
24. Bertolotti A, Zhang YH, Hendershot LM, Harding HP, Ron D: Dynamic interaction of Bip and ER stress transducers in the unfolded protein response. *Nat Cell Biol* 2:326–332, 2000
25. Qu L, Huang S, Baltzis D, Rivas-Estilla AM, Pluquet O, Hatzoglou M, Koumenis C, Taya Y, Yoshimura A, Koromilas AE: Endoplasmic reticulum stress induces p53 cytoplasmic localization and prevents p53-dependent apoptosis by a pathway involving glycogen synthase kinase-3 beta. *Genes Dev* 18:261–277, 2004
26. Harding HP, Ron D: Endoplasmic reticulum stress and the development of diabetes: a review. *Diabetes* 51 (Suppl. 3):S455–S461, 2002